Optical dielectric functions of wurtzite III-V semiconductors

Amrit De and Craig E. Pryor
Department of Physics and Astronomy and Optical Science and Technology Center, University of Iowa, Iowa City, Iowa 52242, USA
(Received 16 November 2010; revised manuscript received 4 March 2011; published 13 March 2012)

Optical properties of semiconductors can exhibit strong polarization dependence due to crystalline anisotropy. A number of recent experiments has shown that the photoluminescence intensity in free standing nanowires is polarization dependent. One contribution to this effect is the anisotropy of the dielectric function due to the fact that most nanowires crystalize in the wurtzite form. While little is known experimentally about the band structures of wurtzite phase III-V semiconductors, we have previously predicted the bulk band structure of nine III-V semiconductors in the wurtzite phase. Here, we predict the frequency dependent dielectric functions for nine non-nitride wurtzite phase III-V semiconductors (AlP, AlAs, AlSb, GaP, GaAs, GaSb, InP, InAs, and InSb). Their complex dielectric functions are calculated in the dipole approximation for light polarized parallel and perpendicular to the *c* axis of the crystal. Momentum matrix elements are evaluated on a dense grid of special *k* points using empirical pseudopotential wave functions. Corrections to the momentum matrix elements, to account for the missing core states, are made using a scaling factor which is determined from the zinc-blende polytypes. Simple analytic expressions are provided for the dispersion relations in the vicinity of the respective fundamental absorption edges.

DOI: 10.1103/PhysRevB.85.125201 PACS number(s): 78.20.Ci, 71.20.−b, 71.15.Dx

I. INTRODUCTION

Frequency-dependent reflectivity and absorption spectra have been a fundamental tool for studying the band structures of semiconductors. In semiconductors with wurtzite (WZ) structure, the optical properties are very strongly polarization dependent[1–6] due to the crystalline anisotropy. The optical selection rules for WZ[7,8] dictate which polarization dependent interband transitions are allowed. This helps in further resolving the band structure for WZ and is used to determine crystal-field splitting and spin-orbit splitting energies.

A number of recent experiments have measured the optical polarization dependent photoluminescence(PL) intensity in free standing nanowires.[9–15] These results reveal a very strong polarization dependence in the PL intensity depending on whether the incident light is polarized parallel or perpendicular to the growth axis of the nanowire. This polarization anisotropy has been attributed to effects, such as heavy- and light-hole mixing,[16] a large dielectric contrast between the nanowires and their surroundings,[9] and the intrinsic band structure properties of the nanowires.[17]

It is well known that III-V semiconductor nanowires easily tend to crystalize in the WZ phase rather than in the zinc blende(ZB) (which is the more stable phase for non-nitride bulk III-Vs). In general, semiconductors can crystallize in their non-naturally occurring phase under extreme thermodynamic conditions. For example, WZ phase diamond (Lonsdalite) can be synthesized directly from cubic diamond using rapid shock wave compression.[18] Similarly hexagonal phases of Si and Ge can be observed under high pressure as well.[19,20] III-V semiconductors typically tend to crystalize either in β-Sn, nickeline (NiAs), or rocksalt structures when subjected to high temperature and pressure. Their occurrence in the bulk WZ phase has been rare with the exception of a recent experiment in which bulk WZ phase GaAs was synthesized.[21] However when grown as a nanowire, III-V semiconductors tend to crystalize in the WZ phase. Several theoretical explanations have been proposed for the nanowire's WZ structure. It has been attributed to factors such as small nanowire radii,[22,23] growth kinetics,[24] interface energies,[25] and electron accumulation at the catalyst's interstitial site.[26]

As the non-nitride III-V semiconductor nanowires tend to crystalize in the WZ phase rather than the stable bulk ZB phase, it is likely that their observed polarization dependent optical anisotropy is partly due to its WZ crystal structure. However, bulk WZ phase III-V semiconductors do not naturally occur. Hence, without bulk samples it is not possible to determine the optical properties with traditional absorption and emission measurements.

In Ref. 27 we predicted the bulk band structure of nine non-nitride III-V semiconductors in the WZ phase using empirical pseudopotentials, including SO interactions. These calculations were based on transferable model pseudopotentials assuming ideal relations between the ZB and WZ phases and their lattice constants. The spherically symmetric ionic model potentials for the ZB phase were first obtained by fitting the calculated transition energies to experimental transition energies at high symmetry points. The WZ phase band structures were then obtained by transferring the model ionic pseudopotentials to the WZ pseudopotential Hamiltonian. This is justified because in both ZB and WZ, all of the nearest neighbors and nine out of the twelve second nearest neighbors are at identical crystallographic locations,[28] while all the second nearest neighbors are equidistant. This method has proven to be quite successful in the past, in obtaining band structures of various polytypes.[29–33] Our agreement with experiment was excellent for the known band gaps of InP, InAs, and GaAs. As the empirical pseudopotential method provides an accurate description of the band structure of semiconductors, it can also explain much of the observed intraband and interband transitions in the optical absorption spectra.[33,34]

Note that in general pseudopotential form factors can be obtained in two different ways—empirically (where the form factors are adjusted to match experiment) and from first principles methods. In the case of *ab-initio* methods, there

 ©2012 American Physical Society

are no adjustable parameters *per se*, however the calculated structural, electronic, and vibrational properties can vary substantially depending on the choice of functionals.[35–38] Most first principles methods have well known shortcomings when it comes to predicting band structures. Empirical pseudopotential methods (EPMs) are therefore quite advantageous in this regard, and in addition they are also well suited for large supercell calculations.

In this article, we predict the frequency dependent linear dielectric function for the WZ phase of nine III-V semiconductors, based on our previous empirical pseudopotential band structure calculations.[27] The dielectric functions are calculated in the linear optical response regime within the electric dipole approximation. The required momentum matrix elements are obtained by using the calculated wave functions from our previous calculations.[27]

In general, the momentum Matrix elements need to be corrected as the pseudo-wave-functions do not include the core states. Such corrections have been made using nonlocal correction terms.[39–42] Nonlocal corrections can also be included to account for exchange and correlations effects which can lead to improvements in the calculated optical properties.[43–45] For our calculations nonlocal effects are included in the form of spin orbit interactions. Since the optical spectra of the ZB phase of the III-Vs are already known, we make additional corrections to the optical spectra by using the optical sum rules to correct the static dielectric function ϵ_0. Since the core states of the constituent elements of the two polytypes is the same, corrections to account for the missing core states should be the same for both ZB and WZ forms. By using the optical sum rules, a set of constants can be obtained which normalizes the calculated ZB ϵ_0 to experimental ZB values. These normalization constants are then transferred to their respective WZ polytypes which then account for corrections to their dielectric functions.

Our calculations are carried out within the one-particle picture to help interpret the polarization dependence of the nanowires. Much work has been done in recent years to include the effects of electron-hole interactions in the dielectric function.[46–52] For many *first principles* calculations, it has been seen that the two particle contributions improve agreement with experiment for the low energy part of the optical spectrum of semiconductors, mostly by readjusting the heights of the $E1$ and $E2$ peaks.[46] While these corrections help to fine tune the dielectric spectrum's agreement with experiment for many materials, the dominant contribution to the dielectric function comes from one-particle calculations, which by themselves are in very good agreement with experiment in many instances.[53–55] Moreover, as dielectric functions calculated in the single particle picture using the empirical pseudopotential method are in far better agreement with experiment than ones using *ab-initio* methods,[33] perturbative corrections can be seen to be less important for single particle EPM calculations. Often times, the static dielectric function is overestimated in *ab-initio* calculations[56–58] and can be improved upon by the inclusion of local field effects.[47] However, these steps are not necessary for our calculations as we are using a maximally constrained EPM, in which our calculated static dielectric constant (in ZB phase) is normalized to experiment, thus taking any constant correction for ϵ_0 into account. Local field effects can shift peak positions,[48] which improves *ab-initio* calculations which suffer from discrepancies in excited state energies. However, such corrections could have spurious effects for optical properties calculated using EPMs.

This paper is organized as follows. In Sec. II, a brief theoretical background of the optical properties is presented along with our method for the calculations. The calculated dielectric functions and reflectivity spectra are presented in Sec. III along with our tabulated results for ϵ_0. This is followed by a brief discussion and summary. For the sake of completeness, we also list some key details of our band structure calculations from Ref. 27 in the Appendix.

II. OPTICAL PROPERTIES

Consider a semi-infinite crystal having a symmetry equivalent to or higher than that of the orthorhombic crystal system. If we choose our coordinate such that the z axis is the surface normal and the x-z plane is the plane of incidence, then the reflectivity for light polarized perpendicular to the plane of incidence is given by[59,60]

$$R_s = \left| \frac{\cos\theta - \left(n_y^2 - \sin^2\theta\right)^{\frac{1}{2}}}{\cos\theta + \left(n_y^2 - \sin^2\theta\right)^{\frac{1}{2}}} \right|^2, \tag{1}$$

where θ at an angle of incidence. Similarly the reflectivity for light polarized parallel to the plane of incidence is

$$R_p = \left| \frac{n_x n_z \cos\theta - \left(n_z^2 - \sin^2\theta\right)^{\frac{1}{2}}}{n_x n_z \cos\theta + \left(n_z^2 - \sin^2\theta\right)^{\frac{1}{2}}} \right|^2, \tag{2}$$

where n_x, n_y and n_z are the complex indices of refraction. In the case of an optically uniaxial crystal, such as WZ, if the surface normal is parallel to the c axis, then $n_z = n_{||}$ and $n_x = n_y = n_\perp$. The linear refractive index $n(\omega) = \sqrt{\epsilon(\omega)}$, where the dielectric function can be written as

$$\epsilon(\omega) = \epsilon'(\omega) + i\epsilon''(\omega). \tag{3}$$

In the linear response regime, the real and imaginary parts of the dielectric function are related to each other by the Kramers-Kronig (KK) relations

$$\epsilon'(\omega) = 1 + \frac{2}{\pi}\mathcal{P}\int_0^\infty \frac{\omega'\epsilon''(\omega)}{\omega'^2 - \omega^2} d\omega', \tag{4}$$

$$\epsilon''(\omega) = -\frac{2}{\pi}\mathcal{P}\int_0^\infty \frac{\omega\epsilon'(\omega)}{\omega'^2 - \omega^2} d\omega', \tag{5}$$

where $\mathcal{P}$ is the Cauchy principle value.

For obtaining optical properties of the WZ semiconductors, we first evaluate $\epsilon''(\omega)$ using our empirical pseudopotential band structure calculations of Ref. 27 (also see the Appendix). The real part $\epsilon'(\omega)$ is numerically obtained using Eqs. (4) and (5) is used to check for self consistency. In the electric dipole approximation, assuming only direct band to band transitions are allowed between an initial state i and a final state j, $\epsilon''(\omega)$ is given by

$$\epsilon''(\omega) = \left(\frac{\hbar\pi^2 e^2}{m^2\omega^2}\right) \sum_{ij} \int_{BZ} |M_{ij}|^2 \delta(E_{c,j}(\mathbf{k}) - E_{v,i}(\mathbf{k}) - \hbar\omega) d^3k, \tag{6}$$

where $\int_{BZ}$ is an integration over the entire Brillouin zone (BZ), $\sum_{ij}$ is a sum over all initial valence band and final conduction band states, and $E_v(\mathbf{k})$ and $E_c(\mathbf{k})$ are the valence and conduction band energies at their respective $\mathbf{k}$'s. For the delta function, we use

$$\delta(\Delta E - \hbar\omega) \approx \frac{2}{1 + \cosh[\gamma(\Delta E - \hbar\omega)]}, \tag{7}$$

where γ is an adjustable damping parameter that can be used to incorporate lifetime broadening effects. We used $\gamma = 100\ \mathrm{eV}^{-1}$ which gives a transition linewidth of about 35 meV.[61] The momentum matrix elements M_{ij} for interband transitions are obtained from the pseudo-wave-functions from our empirical pseudopotentials for WZ,[27] given by

$$\phi_{\mathbf{k}}(\mathbf{r}) = \sum_{\mathbf{G}} c(\mathbf{k},\mathbf{G}) \exp[i(\mathbf{k} + \mathbf{G}) \cdot \mathbf{r}], \tag{8}$$

where $c(\mathbf{k},\mathbf{G})$ are the eigenvector coefficients at a given $\mathbf{k}$. The momentum matrix element between the states i and j is

$$M_{ij}(\mathbf{k}) = \langle \phi^i_{\mathbf{k}} | \hat{p} | \phi^j_{\mathbf{k}} \rangle, \tag{9}$$

where $\hat{p}$ is the momentum operator. Using Eq. (8), M_{ij} can be rewritten in terms of the expansion coefficients as

$$M_{ij}(\mathbf{k}) = i \sum_{\mathbf{G}} c^*_i(\mathbf{k},\mathbf{G}) c_j(\mathbf{k},\mathbf{G}) [(\mathbf{k} + \mathbf{G}) \cdot \hat{\mathbf{e}}], \tag{10}$$

where $\hat{\mathbf{e}}$ is the polarization vector. The expansion coefficients, c_i and c_j, are the eigenvectors of ith and jth states in the pseudopotential Hamiltonian. $\epsilon''(\omega)$ is then calculated using Eqs. (5), (6), and (10) for light polarized parallel and perpendicular to the c axis. In practice, it is difficult to explicitly evaluate the Brillouin zone integral in Eq. (6) because of the prohibitively large number of k values that would be required. However, integration schemes that allow the BZ integral to be replaced by a sum over a set of special k points can be used. We have used a set of 4.5×10^4 special k points based on the scheme of Monkhorst and Pack.[62]

Momentum matrix elements calculated using the pseudo-wave-functions must be corrected since the pseudo-wave-functions do not include the core states. One method is to include the commutator of the nonlocal pseudopotential and the position operator,[63,64] while Kageshima and Shiraishi have proposed correcting the momentum matrix elements by including a core repair term.[39] Both techniques cause small changes in the dielectric function. Monachesi *et al.* have compared the dielectric functions of GaAs calculated with *ab-initio* pseudopotential wave functions against calculations with true electron wave functions, and they find virtually no differences due to the missing core states.[42] In our calculations we take advantage of the fact that our pseudopotentials are being transferred between polytypes, and hence any core corrections should be nearly identical. We normalize the calculated $\epsilon(\omega = 0)$ to the experimentally known static dielectric constant by making use of the optical sum rule

$$\epsilon_o = 1 + C' \frac{2}{\pi} \int_0^\infty \frac{\epsilon''(\omega) d\omega}{\omega}, \tag{11}$$

where C' is a scaling constant which is determined as follows. First the dielectric functions for all the ZB phase

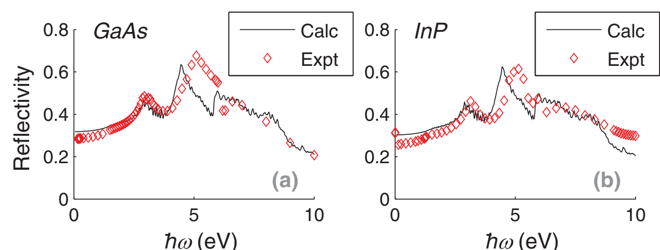

FIG. 1. (Color online) Comparison between calculated and measured reflectivity spectra at normal incidence for zinc-blende phase (a) GaAs and (b) InP.

semiconductors are evaluated using empirical pseudopotential wave functions. The constant C' is then adjusted so that the calculated ϵ_0 for ZB matches experimental values obtained from Ref. 65. By empirically fitting to ϵ_0, this method results in good agreement between theory and experiment for frequencies $\omega > 0$. As an example, we show a comparison between the calculated and measured reflectivity spectra at normal incidence for cubic GaAs and InP in Fig. 1. The measured dielectric functions for GaAs and InP were obtained from Ref. 66.

For the WZ calculations, $\epsilon''_\perp$ and $\epsilon''_{||}$ obtained using Eq. (6) are multiplied by the same scaling constant C'. We expect this method to yield good results for the WZ semiconductors since both polytypes consist of the same atomic species; so the corrections to account for missing core states will be the same.

III. RESULTS AND DISCUSSION

The calculated ϵ_0 for light polarized parallel and perpendicular to the c axis are listed in Table I. The values listed in the table show that generally, materials with heavier elements have larger static dielectric constants. We also see that $\epsilon_0^\perp < \epsilon_0^{||}$ in the case of GaAs, GaSb, and InSb, whereas $\epsilon_0^\perp > \epsilon_0^{||}$ for AlP, AlAs, GaP, InP, and InAs.

For WZ materials, with the inclusion of spin-orbit interactions, all zone center states belong to either a Γ_7, Γ_8, or Γ_9 representation (all in double group notation). The zone center conduction band minima have either Γ_7 or Γ_8 symmetry, and the valence band states are the Γ_9 heavy hole, Γ_7^1 light hole, and a Γ_7 splitoff hole. The interband transitions for WZ are dictated by the polarization dependent optical selection

TABLE I. Calculated static dielectric constants for light polarized parallel and perpendicular to the c axis, for nine WZ phase III-V semiconductors.

Material	$\epsilon_0^\perp$	$\epsilon_0^{\|\|}$
AlP	10.464	8.232
AlAs	10.853	9.165
AlSb	12.056	11.933
GaP	11.708	10.223
GaAs	12.481	13.066
GaSb	15.215	17.621
InP	12.812	10.435
InAs	16.782	13.610
InSb	16.952	19.379

rules.[7,8] For light polarized parallel to the c axis ($E_{||}$), only transitions between states with the same symmetry are allowed, i.e., $\Gamma_7 \leftrightarrow \Gamma_7$, $\Gamma_8 \leftrightarrow \Gamma_8$, and $\Gamma_9 \leftrightarrow \Gamma_9$. For light polarized perpendicular to the c axis($E_{\perp}$), the allowed transitions are $\Gamma_7 \leftrightarrow \Gamma_7$, $\Gamma_8 \leftrightarrow \Gamma_8$, $\Gamma_9 \leftrightarrow \Gamma_7$, and $\Gamma_9 \leftrightarrow \Gamma_8$. Note that the $\Gamma_7 \leftrightarrow \Gamma_8$ transition is forbidden for all polarizations.

The other high symmetry k-point transitions allowed for $E_{||}$ are $A_{7,8} \leftrightarrow A_{7,8}$, $A_9 \leftrightarrow A_9$, $K_{4,5} \leftrightarrow K_{4,5}$, $K_6 \leftrightarrow K_6$, $H_{4,5} \leftrightarrow H_{4,5}$, and $H_6 \leftrightarrow H_6$. For $E_{\perp}$ the allowed dipole transitions are $A_{7,8} \leftrightarrow A_{7,8}$, $A_9 \leftrightarrow A_{7,8}$, $K_{4,5} \leftrightarrow K_6$, and $H_{4,5} \leftrightarrow H_6$. The M and L point transitions (i.e., $M_5 \leftrightarrow M_5$ and $L_5 \leftrightarrow L_5$) are allowed for all polarizations. For a comprehensive list of optical selection rules for WZ at various high symmetry points and along various directions, see Refs. 8 and 67.

The zone center transition energies for the first thirteen states and their respective irreducible representations are listed in Ref. 27. Our band structure calculations show that the indirect gap ZB semiconductors (AlP, AlAs, AlSb, and GaP) have direct band gaps in the WZ phase[27] with Γ_8 conduction band minima. These materials will be partially optically active, with transitions from the Γ_9 heavy-hole bands allowed for $E_{\perp}$, making them technologically important. The other semiconductors with Γ_8 conduction band minima in the WZ phase are GaAs and GaSb. The indium containing WZ semiconductors all have direct band gaps with Γ_7 conduction band minima and are optically active for all polarizations of the electric field.

The calculated $\epsilon'(\omega)$ and $\epsilon''(\omega)$ for light polarized parallel and perpendicular to the c axis for the nine III-V semiconductors of interest are shown in Figs. 2–4 The corresponding

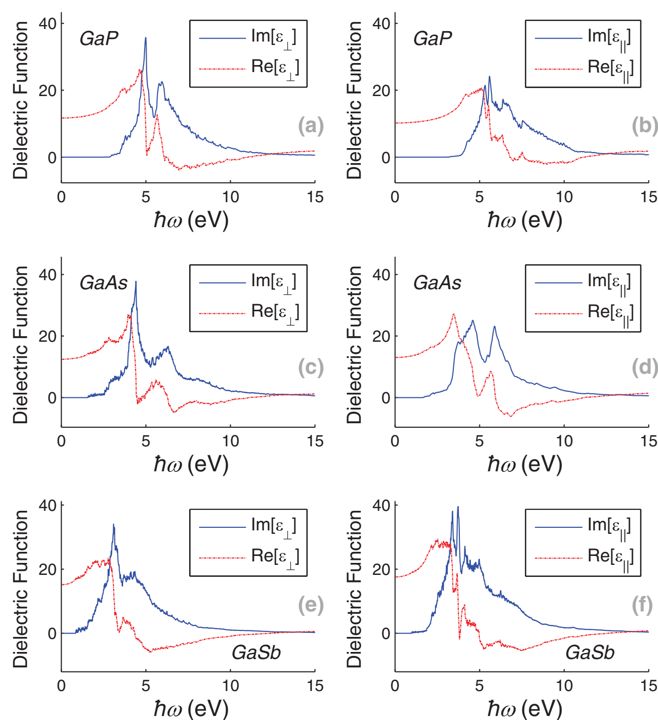

FIG. 3. (Color online) Real and imaginary parts of the complex dielectric function as a function of incident photon energies and polarizations for (a) $E_{\perp}$ in GaP, (b) $E_{||}$ in GaP, (c) $E_{\perp}$ in GaAs, (d) $E_{||}$ in GaAs, (e) $E_{\perp}$ in GaSb, and (f) $E_{||}$ in GaSb.

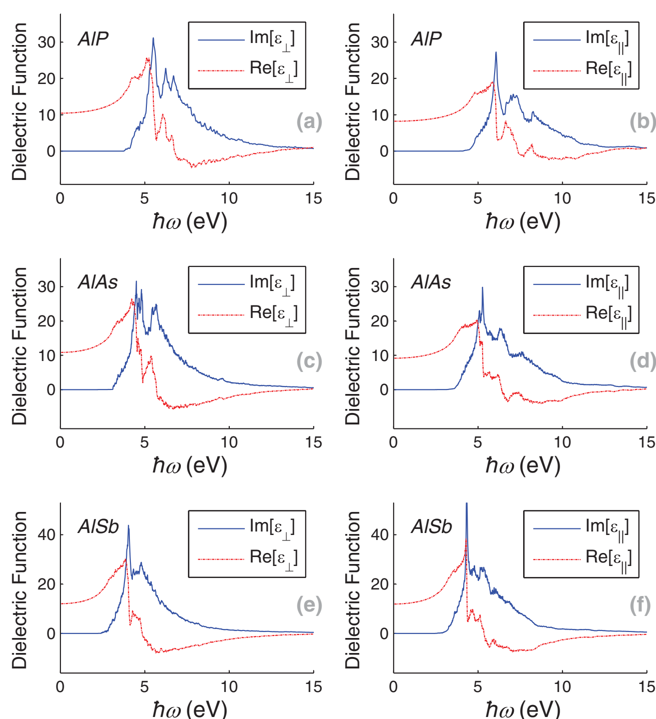

FIG. 2. (Color online) Real and imaginary parts of the complex dielectric function as a function of incident photon energies and polarizations for (a) $E_{\perp}$ in AlP, (b) $E_{||}$ in AlP, (c) $E_{\perp}$ in AlAs, (d) $E_{||}$ in AlAs, (e) $E_{\perp}$ in AlSb, and (f) $E_{||}$ in AlSb.

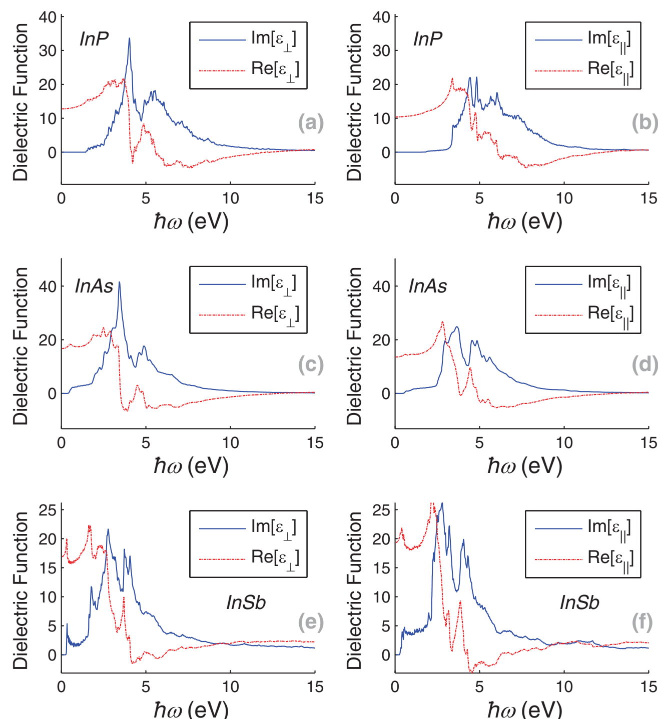

FIG. 4. (Color online) Real and imaginary parts of the complex dielectric function as a function of incident photon energies and polarizations for (a) $E_{\perp}$ in InP, (b) $E_{||}$ in InP, (c) $E_{\perp}$ in InAs, (d) $E_{||}$ in InAs, (e) $E_{\perp}$ in InSb, and (f) $E_{||}$ in InSb.

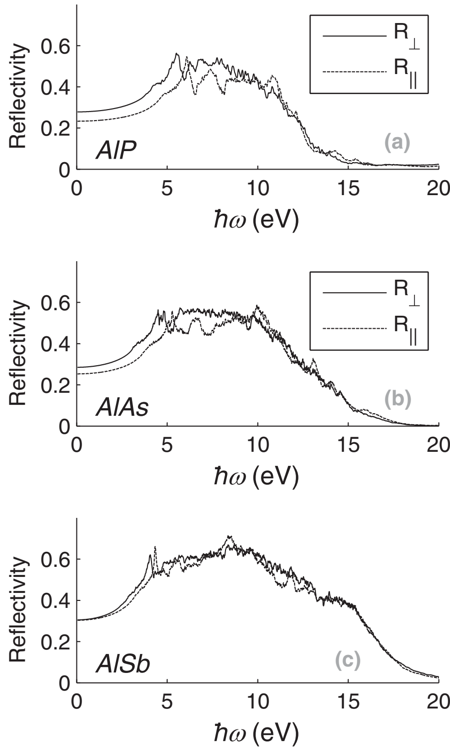

FIG. 5. Calculated reflectivity spectra at normal incidence for (a) AlP, (b) AlAs, and (c) AlSb.

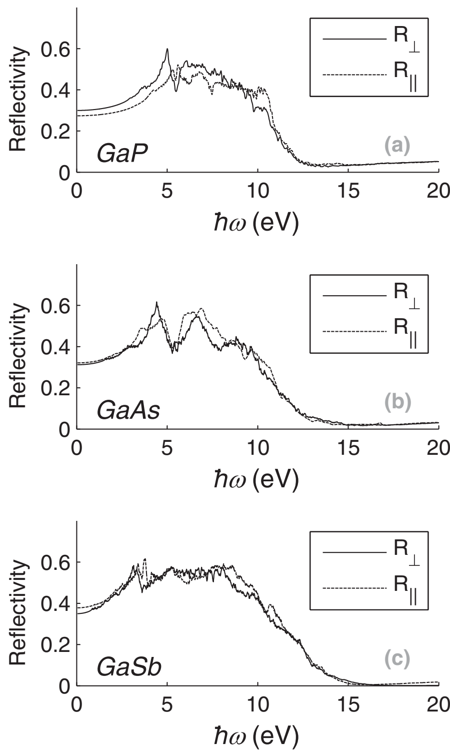

FIG. 6. Calculated reflectivity spectra at normal incidence for (a) GaP, (b) GaAs, and (c) GaSb.

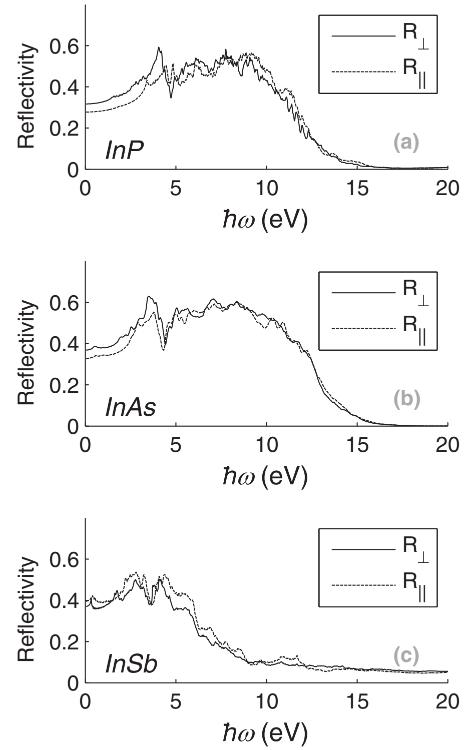

FIG. 7. Calculated reflectivity spectra at normal incidence for (a) InP, (b) InAs, and (c) InSb.

reflectivity spectra for both polarizations are shown in Figs. 5–7. The reflectivity spectra for the different WZ crystals are distinct and depend on the details of their electronic band structure. For the WZ semiconductors, the most prominent features are typically seen up to about 7 eV. As expected, all the WZ phase semiconductors exhibit optical anisotropy, the degree of which varies with the semiconductor. The reflectivity spectra for the two different polarizations shows several peaks which originate from interband transitions along various high symmetry points.

In order to illustrate the the dielectric function's variations about the fundamental absorption edge (FAE), we fit the numerically calculated $\epsilon_\perp$ and $\epsilon_{||}$ (in the vicinity of their respective band gaps) to the Lorentz oscillator model. The real and imaginary parts of which are

$$\epsilon'(\omega) = 1 - f \sum_{j=1}^{2} \frac{\omega^2 - \Omega_j^2}{\left(\omega^2 - \Omega_j^2\right)^2 - (\Gamma_j \omega)^2}, \tag{12}$$

$$\epsilon''(\omega) = f \sum_{j=1}^{2} \frac{\Gamma_j \omega}{\left(\omega^2 - \Omega_j^2\right)^2 - (\Gamma_j \omega)^2}, \tag{13}$$

where f, Ω_j, and Γ_j were used as fitting parameters and are listed in Table II. Typically, f is the oscillator strength, Γ_j is a relaxation rate and Ω_j is a resonance frequency term. Note that the real and imaginary parts of the dielectric functions were separately fit to Eqs. (12) and (13).

These fits in terms of the Lorentz oscillators provides an analytical expression for the dielectric function's dispersion relations, which could be useful for designing optical devices. Note that the dispersion relations for different materials are

TABLE II. Fit coefficients for the dielectric constants for the III-V WZ semiconductors about their respective band gaps. $\hbar\omega_K$ is the upper cutoff energy up until which these fits are valid.

		For $\epsilon'_{\perp}$					For $\epsilon''_{\perp}$					For $\epsilon'_{\parallel}$					For $\epsilon''_{\parallel}$				
Material	$\hbar\omega_K$ (eV)	f	Ω_1	Γ_1	Ω_2	Γ_2	f	Ω_1	Γ_1	Ω_2	Γ_2	f	Ω_1	Γ_1	Ω_2	Γ_2	f	Ω_1	Γ_1	Ω_2	Γ_2
AlP	4	130.1	5.639	6.064	4.927	-0.7225	1.062	2.075	-9.482×10^{-6}	4.059	0.2963	137.3	6.702	7.095	5.742	8.292×10^{-6}	0.3597	2.045	-4.889×10^{-6}	4.374	0.2395
AlAs	3.5	98.66	5.281	7.39	3.945	-0.7937	6.019	1.775	-1.505×10^{-5}	3.525	0.3752	111	5.818	5.958	4.774	1.94×10^{-5}	0.3517	1.775	-1.349×10^{-5}	3.564	0.3594
AlSb	3.5	173.3	24.43	1048	4.006	-0.9518	29.01	1.775	-2.341×10^{-5}	3.574	0.6396	123.5	6.17	8.954	4.006	-0.7481	10.49	1.775	-1.476×10^{-5}	3.605	0.4174
GaP	4	214.4	13.87	104.8	4.715	-1.357	18.66	2.045	-2.168×10^{-5}	4.011	0.6816	142.9	6.11	6.582	5.157	-3.88×10^{-6}	5.39	2.045	-8.046×10^{-6}	4.257	0.3438
GaAs	2.5	35.06	2.279	1.548	2.781	0.3765	6.239	1.295	-0.0002109	2.064	0.9754	160.6	22.74	666.6	3.696	1.721	2.93	1.295	-5.471×10^{-5}	2.515	0.6727
GaSb	1.5	21.1	1.652	1.416	1.825	0.3051	109.5	0.7851	-3.005×10^{-6}	2.201	0.0881	46.47	2.319	2.244	2.424	0.0002	0.4912	0.7852	-0.0001	1.488	0.6783
InP	2.5	43.84	2.616	1.958	2.89	0.4301	14.99	1.295	-4.324×10^{-5}	2.962	1.289	74.09	3.942	3.117	4.005	-9.183×10^{-5}	1.076	1.295	-6.656×10^{-5}	2.502	0.8105
InAs	1	10.68	1.079	0.9922	1.269	0.2729	2.157	0.5467	7.456×10^{-5}	1.042	0.7514	9.755	1.186	1.171	1.319	-0.3299	1.332	0.5424	-5.915×10^{-5}	1.17	0.7103
InSb	0.5	2.54	0.5128	0.429	0.6435	-0.1199	0.3746	0.2754	-0.0012	0.414	0.2541	3.401	0.5733	0.4854	0.6665	-0.1552	0.7352	0.2748	-0.0003	0.5696	0.2978

valid only within a certain cutoff frequency (ω_K as given in Table II). This cutoff frequency indicates the region within which the dispersion relation is smooth. The fitting parameters (fs, Γ_i's, and Ω_i's) depend on ω_K and as such are not necessarily representative of the trends in the optical properties of the III-V semiconductors.

In general, we find that the fitting parameter f is greater for $\epsilon''_{\perp}$ than for $\epsilon''_{\parallel}$. Based on optical selection rules, this can be explained by the fact that for $E_{\perp}$ a transition between the Γ_9 heavy hole (HH) and the Γ_7 (or Γ_8) conduction band (CB) is allowed. Hence the FAE is at the band gap (E_g). For $E_{\parallel}$ the allowed transition with the lowest energy will be between the Γ_7 light hole (LH) and Γ_7. As a result for $E_{\parallel}$, InP, InAs, and InSb, the FAE will be at $E_g + \Delta_1$, where Δ_1 is the energy difference between the Γ_9 heavy hole and Γ_7 light hole. In general, indium containing compounds have prominent features in the reflectivity spectra near the FAE as a number of valence band to conduction band transitions are allowed. In all others (AlP, AlAs, AlSb, GaP, GaAs, and GaSb), no noticeable sharp features are seen in the vicinity of the FAE since they all have Γ_8 CBs, and the optical selection rules forbid transitions from the LH and the splitoff hole for all polarizations and from the HH for $E_{\parallel}$.

The spin-orbit coupling can alter the ordering of the valence band states in different WZ semiconductors. In our calculations, the valence band states in all materials except InSb have normal ordering (i.e, Γ_9, Γ_7, Γ_7[7,68]). The ordering of the valence band states in InSb is complicated by the very large spin-orbit splitting which forces the Γ_7 splitoff hole below the next Γ_9 state, resulting in the unusual Γ_9, Γ_7, Γ_9, Γ_7 valence band ordering. Attempts to optically measure the spin-orbit splitting energy in the WZ type InSb could be complicated by this.

IV. SUMMARY

In summary we have calculated the optical properties of AlP, AlAs, AlSb, GaP, GaAs, GaSb, InP, InAs, and InSb in the WZ phase using empirical pseudopotentials. Their complex dielectric function was evaluated as a function of incident photon energy up to 20 eV for light polarized parallel and perpendicular to the c axis. The dielectric functions were calculated in the dipole approximation by evaluating the optical momentum matrix elements using empirical pseudopotential wave functions (from Ref. 27) on a grid of about 4.5×10^4 special k points. Corrections to the pseudo-momentum-matrix elements to account for the missing core states are introduced via a scaling factor, which is determined from the ratio of the calculated to measured static dielectric function for the corresponding zinc-blende polytypes. The reflectivity spectra for all nine WZ semiconductors was also calculated for both polarizations and was seen to exhibit optical anisotropy as well. Finally, for each material the frequency dependent dielectric function was fit to a Lorentz oscillator model in the vicinity of the fundamental absorption edge, providing a simple analytic expression for the dispersion relation.

In general it is seen that most of the III-V semiconductors exhibit strong optical anisotropy. This suggests that among other applications, these WZ semiconductors could find potential use in nonlinear optics. For applications, such as optical frequency conversion, nonlinear optical crystals have to

be optically birefringent to satisfy phase matching conditions. ZB phase III-V semiconductor crystals are not particularly useful in this regard as they are optically isotropic whereas the non-nitride WZ III-Vs are optically birefringent. This can lead to a whole new class of nonlinear optical crystals.

APPENDIX

Here we present the details of our band structure calculations of the WZ phase of III-V semiconductors from Ref. 27. Our band structure calculations closely followed the empirical pseudopotential formalism of Cohen and Chelikowsky.[33] However, rather than using discrete form factors we have used continuous model potentials so that it is applicable to both ZB and WZ structures. The pseudopotential Hamiltonian consists of the kinetic, local pseudopotential, and SO interaction terms:

$$H = \frac{-\hbar^2\mathbf{K}^2}{2m} + V_{pp} + V_{so}. \tag{A1}$$

The position dependent local pseudopotential V_{pp} and nonlocal SO interaction term V_{so} can be expanded in terms of the reciprocal lattice vectors $\mathbf{G}$. In case of binary compounds, the local pseudopotential can be separated into symmetric (S) and antisymmetric (A) parts,

$$\langle \mathbf{G}'|V_{pp}|\mathbf{G}\rangle = V^S(\mathbf{G}'-\mathbf{G})S^S(\mathbf{G}'-\mathbf{G}) + iV^A(\mathbf{G}'-\mathbf{G})S^A(\mathbf{G}'-\mathbf{G}), \tag{A2}$$

where the symmetric and antisymmetric structure factors are given by $S^S(\mathbf{G}) = \sum_j \exp(-i\mathbf{G}\cdot\boldsymbol{\tau}_j)/N$ and $S^A(\mathbf{G}) = -i\sum_j P_j \exp(-i\mathbf{G}\cdot\boldsymbol{\tau}_j)/N$. Here N is the number of atoms per unit cell, and $\boldsymbol{\tau}_j$ is the basis vector of the jth atom in the unit cell. $P_j = +1$ for one type of atom and -1 for the other type. With type-1 atoms located at (0,0,0) and $\frac{2}{3}\mathbf{a}_1 + \frac{1}{3}\mathbf{a}_2 + \frac{1}{2}\mathbf{a}_3$ and the type-2 atoms are located at $u\mathbf{a}_3$ and $\frac{2}{3}\mathbf{a}_1 + \frac{1}{3}\mathbf{a}_2 + (\frac{1}{2}+u)\mathbf{a}_3$, the WZ structure factors are

$$S^S(\mathbf{G}) = \tfrac{1}{4}(1+e^{-iG_zuc})(1+e^{-iG_ya/\sqrt{3}+G_zc/2}), \tag{A3}$$

$$S^A(\mathbf{G}) = \tfrac{1}{4}(1-e^{-iG_zuc})(1+e^{-iG_ya/\sqrt{3}+G_zc/2}), \tag{A4}$$

where G_y and G_z are the y and z components of $\mathbf{G}$, $\mathbf{a}_1 = (1,\sqrt{3},0)a/2$, $\mathbf{a}_2 = (1,-\sqrt{3},0)a/2$, and $\mathbf{a}_3 = (0,0,c)$ are primitive lattice vectors. Here a and c are WZ lattice constants and $u = a/c$.

The symmetric $V^S(\mathbf{G})$ and antisymmetric form factors $V^A(\mathbf{G})$ are formed from the sum and difference of the spherically symmetric anion and cation potentials. In the empirical pseudopotential approach, the form factors are adjusted to fit the calculated energy spectrum to experiment. We took $V^S(\mathbf{G})$ and $V^A(\mathbf{G})$ to be continuous functions of $\mathbf{G}$ using model potentials of the form[69–71]

$$V^S(\mathbf{G}) = \frac{x_1G + x_2}{\exp(x_3G^2 + x_4) + 1}, \tag{A5}$$

$$V^A(\mathbf{G}) = x_1'G^2 + x_2'\exp(x_3'G^2 + x_4'), \tag{A6}$$

where $G = |\mathbf{G}|a/2\pi$ is a dimensionless number. The parameters x_j and x_j' were first adjusted to fit the calculated ZB band structure to experimental transition energies (see Table III for a list of fitting parameters). The WZ pseudopotential for a given binary compound is then constructed by combining these spherically symmetric atomic form factors with the appropriate structure factors for WZ [see Eq. (A2)].

For the SO interaction term we considered core shells filled up to the d orbitals (depending on the valence shells of the constituent elements of the III-V semiconductors). The matrix elements for the SO interaction term in a binary compound are

$$\begin{aligned}\langle \mathbf{K}',s'|V_{so}|\mathbf{K},s\rangle = &-i(\hat{\mathbf{K}}'\times\hat{\mathbf{K}})\cdot\langle s'|\boldsymbol{\sigma}|s\rangle \\ &\times\{[\lambda_p^S + (\hat{\mathbf{K}}'\cdot\hat{\mathbf{K}})\lambda_d^S]S^S(\mathbf{G}'-\mathbf{G}) \\ &+[\lambda_p^A + (\hat{\mathbf{K}}'\cdot\hat{\mathbf{K}})\lambda_d^A]S^A(\mathbf{G}'-\mathbf{G})\},\end{aligned} \tag{A7}$$

where $\mathbf{K} = \mathbf{G} + \mathbf{k}$, $\boldsymbol{\sigma}$ is a triad of Pauli spin matrices and s,s' are eigenstates of σ_z. Here the symmetric and antisymmetric contributions to the spin-orbit Hamiltonian are defined by

$$\lambda_l^S = (\lambda_l^{(1)} + \lambda_l^{(2)})/2, \tag{A8}$$

$$\lambda_l^A = (\lambda_l^{(1)} - \lambda_l^{(2)})/2, \tag{A9}$$

$$\lambda_l^{(1)} = \mu_l\beta_{nl}^{(1)}(\mathbf{K}_i)\beta_{nl}^{(1)}(\mathbf{K}_j), \tag{A10}$$

$$\lambda_l^{(2)} = \gamma_l\mu_l\beta_{nl}^{(2)}(\mathbf{K}_i)\beta_{nl}^{(2)}(\mathbf{K}_j), \tag{A11}$$

where γ_l is the ratio of the anion to cation atomic-spin-orbit-splitting energies[72] for a given shell. The overlap integral β_{nl} is constructed from the atomic core wave functions

$$\beta_{nl}(K) = C\int_0^\infty i^l\sqrt{4\pi(2l+1)}\,j_{nl}(Kr)R_{nl}(r)r^2dr, \tag{A12}$$

TABLE III. Lattice constants (a and c) along with the fitting parameters for symmetric and antisymmetric form factors used for the WZ band structure calculations in Ref. 27. The form factors are in units of Ry. μ_1 and μ_2 are the fitting parameters for spin-orbit interactions.

Material	a (Å)	c (Å)	x_1	x_2	x_3	x_4	x_1'	x_2'	x_3'	x_4'	μ_1	μ_2
AlP	3.866	6.313	0.083	−0.579	0.031	−2.586	−0.11	0.9	−0.061	−1.178	0.012	0
AlAs	4.003	6.537	0.062	−0.459	0.027	−2.629	−0.041	1.003	−0.056	−1.693	5.28×10^{-3}	5×10^{-5}
AlSb	4.338	7.085	0.06	−0.412	0.032	−2.548	−0.09	0.17	−0.051	−2.098	7.26×10^{-3}	2.96×10^{-4}
GaP	3.854	6.294	0.085	−0.457	0.04	−2.566	−0.351	5.165	−0.205	0.339	0.385	-2.3×10^{-3}
GaAs	3.997	6.528	0.058	−0.467	0.023	−2.583	−0.063	1.091	−0.074	−1.298	0.052	8.3×10^{-6}
GaSb	4.310	7.039	0.042	−0.343	0.022	−2.584	−0.009	0.618	−0.043	−2.233	0.056	2.78×10^{-5}
InP	4.151	6.778	0.049	−0.385	0.027	−2.602	0	0.847	−0.059	−1.654	0.243	-1.09×10^{-3}
InAs	4.285	6.997	0.036	−0.298	0.033	−2.615	−0.011	1.359	−0.121	−1.124	0.082	2.603×10^{-5}
InSb	4.582	7.482	0.022	−0.174	0.023	−2.42	−0.012	1.158	−0.082	−1.363	0.085	5.7×10^{-5}

TABLE IV. Fit coefficients for $\beta'_{nl}(K)$ for the outermost valence p and d orbital states.

Material	p shell			d shell		
	z_1	z_2	z_3	z_1	z_2	z_3
Al	6.2692	1.5345	6.8611			
P	3.7924	1.4540	4.4142			
Ga	6.3847	1.5446	6.8190	4.3864	1.9159	1.4369
As	4.6614	1.5002	4.6614	73.5331	2.2475	1.2876
In	7.2687	1.6185	7.2687	6.7272	2.1900	1.8123
Sb	5.4336	1.5415	5.2224	30.6479	2.4120	1.6395

where C is a normalization constant such that $\beta_{nl}(K)/K$ approaches unity in the limit K goes to zero, and n is the principal quantum number for the core shell being considered. The radial part of the core wave functions, R_{nl}, was taken from Herman and Skillman tables[73] only for the outermost p and d shells(when applicable). For Ga, In, As, and Sb, terms up to $l = 2$ in Eq. (A7) are considered. Since Al and P do not have valence d shells, the $l = 2$ term (d states) is not included for them. The μ_l's are adjustable parameters which is listed in Table III along with the adjustable parameters for the form factors.

For all atomic species of interest, the overlap integral $\beta_{nl}(K)$ is numerically calculated using Simpson's method as a function of K. This integral can be fit to a curve of the type

$$\beta'_{nl}(K) \approx z_1 K^{z_2} \exp(-z_3 K), \tag{A13}$$

where z_i's are fitting parameters. Using this pre-evaluated form [Eq. (A13)], instead of explicitly calculating the integral in Eq. (A12) at each K, saves a tremendous amount of computational time while giving exactly the same result (to within roundoff error). These fit coefficients in Eq. (A13), z_i, are listed in Table IV for the outermost p and d shells.

For calculating the WZ band structures, the matrix elements of the pseudopotential Hamiltonian need to be obtained in WZ's plane wave basis states. These plane wave basis states are constructed by considering all possible linear combinations of the primitive reciprocal lattice vectors $\mathbf{G} = n_1\mathbf{b}_1 + n_2\mathbf{b}_2 + n_3\mathbf{b}_3$ within a cutoff $|\mathbf{G}|$ (where $n_{1,2,3}$ are integers and $\mathbf{b}_{1,2,3}$ are reciprocal lattice vectors for WZ). The cutoff $|\mathbf{G}|$ is increased until the eigenvalues converge. As compared to ZB, roughly about twice as many plane wave basis states are required for WZ as its primitive unit cell has twice as many atoms as ZB's unit cell.

The calculated electronic and optical properties can noticeably vary depending on the lattice constants. For all our band structure calculations, we assumed an ideal WZ crystal whose lattice constant is related to its ZB counterpart by $a_{WZ} = a_{ZB}/\sqrt{2}$ and $u = 3/8$. The lattice constants used for our calculations are listed in Table III. Relatively little is known about the structure of non-nitride WZ III-V semiconductors. Measurements of bulk samples of metastable WZ GaAs give $u = 0.3693$,[21] while InAs nanowires have an ideal WZ structure with $u = 0.37502$.[74] The scarcity of data for non-nitride III-Vs, and the fact that the one structural measurement in an actual nanowire indicates the ideal structure supports the assumption of an ideal WZ crystal until better data becomes available.

One may also use lattice constants calculated using first principle methods. However, we wish to remark that these lattice constants are often *at least* as far off from the actual experimental values as the ideal lattice constants are. For example in the case of WZ-GaN, the ideal lattice constants ($a = 3.196$ Å and $c = 5.219$ Å) are off by less than 0.5% (averaged error) from experiment ($a = 3.188$ Å and $c = 5.185$ Å), whereas the variouslocal-density-approximation–density-functional-theory (LDA-DFT) lattice constants listed in Refs. 75 and 76 vary between 0.65% to as much as 3%—which is further off from experiment than the ideal lattice constants are.

[1] M. Cardona and G. Harbeke, Phys. Rev. A **137**, 1467 (1965).
[2] D. C. Reynolds, C. W. Litton, and T. C. Collins, Phys. Rev. A **140**, 1726 (1965).
[3] Y.-N. Xu and W. Y. Ching, Phys. Rev. B **48**, 4335 (1993).
[4] S. Ninomiya and S. Adachi, J. Appl. Phys. **78**, 1183 (1995).
[5] T. Kawashima, H. Yoshikawa, S. Adachi, S. Fuke, and K. Ohtsuka, J. Appl. Phys. **82**, 3528 (1997).
[6] A. Alemu, B. Gil, M. Julier, and S. Nakamura, Phys. Rev. B **57**, 3761 (1998).
[7] J. L. Birman, Phys. Rev. **114**, 1490 (1959).
[8] A. H. W. Streitwolf, Phys. Status Solidi B **33**, 225 (1969).
[9] J. Wang, M. S. Gudiksen, X. Duan, Y. Cui, and C. M. Lieber, Science **293**, 1455 (2001).
[10] M. Mattila, T. Hakkarainen, M. Mulot, and H. Lipsanen, Nanotechnol. **17**, 1580 (2006).
[11] M. Mattila, T. Hakkarainen, H. Lipsanen, H. Jiang, and E. I. Kauppinen, Appl. Phys. Lett. **90**, 033101 (2007).
[12] A. Mishra *et al.*, Appl. Phys. Lett. **91**, 263104 (2007).
[13] A. Lan, J. Giblin, V. Protasenko, and M. Kuno, Appl. Phys. Lett. **92**, 183110 (2008).
[14] Y. Kobayashi, M. Fukui, J. Motohisa, and T. Fukui, Physica E **40**, 2204 (2008).
[15] B. V. Novikov, S. Yu. Serov, N. G. Filosofov, I. V. Shtrom, V. G. Talalaev, O. F. Vyvenko, E. V. Ubyivovk, Yu. B. Samsonenko, A. D. Bouravleuv, I. P. Soshnikov, N. V. Sibirev, G. E. Cirlin, and V. G. Dubrovskii, Phys. Status Solidi RRL **4**, 175 (2010).
[16] P. C. Sercel and K. J. Vahala, Phys. Rev. B **42**, 3690 (1990).
[17] M. P. Persson and H. Q. Xu, Phys. Rev. B **70**, 161310 (2004).
[18] H. He, T. Sekine, and T. Kobayashi, Appl. Phys. Lett. **81**, 610 (2002).
[19] G. J. Ackland, Rep. Prog. Phys. **64**, 483 (2001).
[20] A. Mujica, A. Rubio, A. Muñoz, and R. J. Needs, Rev. Mod. Phys. **75**, 863 (2003).
[21] M. I. McMahon and R. J. Nelmes, Phys. Rev. Lett. **95**, 215505 (2005).
[22] T. Akiyama, K. Nakamura, and T. Ito, Phys. Rev. B **73**, 235308 (2006).
[23] M. Galicka, M. Bukala, R. Buczko, and P. Kacman, J. Phys. Condens. Matter **20**, 454226 (2008).
[24] V. G. Dubrovskii and N. V. Sibirev, Phys. Rev. B **77**, 035414 (2008).

[25] F. Glas, J.-C. Harmand, and G. Patriarche, Phys. Rev. Lett. **99**, 146101 (2007).
[26] Y. Haneda, T. Akiyama, K. Nakamura, and T. Ito, Appl. Surf. Sci. **254**, 7746 (2008).
[27] A. De and C. E. Pryor, Phys. Rev. B **81**, 155210 (2010).
[28] J. L. Birman, Phys. Rev. Lett. **2**, 157 (1959).
[29] J. D. Joannopoulos and M. L. Cohen, Phys. Rev. B **7**, 2644 (1973).
[30] S. K. Pugh, D. J. Dugdale, S. Brand, and R. A. Abram, J. Appl. Phys. **86**, 3768 (1999).
[31] G. Pennington and N. Goldsman, Phys. Rev. B **64**, 045104 (2001).
[32] D. Fritsch, H. Schmidt, and M. Grundmann, Appl. Phys. Lett. **88**, 134104 (2006).
[33] M. Cohen and J. R. Chelikowsky, *Electronic Structure and Optical Properties of Semiconductors* (Springer, Berlin, 1988).
[34] *Solid State Physics: Advances in Research and Application*, edited by H. Ehrenreich, F. Seitz, and D. Turnbull (Academic, New York, 1970), Vol. 24.
[35] J. P. Perdew and Y. Wang, Phys. Rev. B **33**, 8800 (1986).
[36] A. D. Becke, Phys. Rev. A **38**, 3098 (1988).
[37] M. Mitani, D. Yamaki, Y. Takano, Y. Kitagawa, Y. Yoshioka, and K. Yamaguchi, J. Chem. Phys. **113**, 10486 (2000).
[38] M. B. Yahia, F. Lemoigno, T. Beuvier, J.-S. Filhol, M. Richard-Plouet, L. Brohan, and M.-L. Doublet, J. Chem. Phys. **130**, 204501 (2009).
[39] H. Kageshima and K. Shiraishi, Phys. Rev. B **56**, 14985 (1997).
[40] B. Adolph, J. Furthmüller, and F. Bechstedt, Phys. Rev. B **63**, 125108 (2001).
[41] C. J. Pickard and F. Mauri, Phys. Rev. B **63**, 245101 (2001).
[42] P. Monachesi, A. Marini, G. Onida, M. Palummo, and R. D. Sole, Phys. Status Solidi A **184**, 101 (2001).
[43] V. I. Gavrilenko and F. Bechstedt, Phys. Rev. B **54**, 13416 (1996).
[44] V. I. Gavrilenko and F. Bechstedt, Phys. Rev. B **55**, 4343 (1997).
[45] W. G. Schmidt, S. Glutsch, P. H. Hahn, and F. Bechstedt, Phys. Rev. B **67**, 085307 (2003).
[46] M. Rohlfing and S. G. Louie, Phys. Rev. Lett. **81**, 2312 (1998).
[47] B. Arnaud and M. Alouani, Phys. Rev. B **63**, 085208 (2001).
[48] G. Onida, L. Reining, and A. Rubio, Rev. Mod. Phys. **74**, 601 (2002).
[49] R. Laskowski, N. E. Christensen, G. Santi, and C. Ambrosch-Draxl, Phys. Rev. B **72**, 035204 (2005).
[50] S. Ismail-Beigi, Phys. Rev. B **77**, 035306 (2008).
[51] T. Puangmali, M. Califano, and P. Harrison, Phys. Rev. B **78**, 245104 (2008).
[52] B. D. Malone, S. G. Louie, and M. L. Cohen, Phys. Rev. B **81**, 115201 (2010).
[53] F. Trani, G. Cantele, D. Ninno, and G. Iadonisi, Phys. Rev. B **72**, 075423 (2005).
[54] I. J. Wu and G. Y. Guo, Phys. Rev. B **76**, 035343 (2007).
[55] L. Makinistian, E. A. Albanesi, N. V. Gonzalez Lemus, A. G. Petukhov, D. Schmidt, E. Schubert, M. Schubert, Y. B. Losovyj, P. Galiy, and P. Dowben, Phys. Rev. B **81**, 075217 (2010).
[56] M. S. Hybertsen and S. G. Louie, Phys. Rev. B **35**, 5585 (1987).
[57] S. de Gironcoli, S. Baroni, and R. Resta, Phys. Rev. Lett. **62**, 2853 (1989).
[58] Z. H. Levine and D. C. Allan, Phys. Rev. B **43**, 4187 (1991).
[59] J. L. P. Mosteller and F. Wooten, J. Opt. Soc. Am. **58**, 511 (1968).
[60] F. Brehat and B. Wyncke, J. Phys. D **24**, 2055 (1991).
[61] C. S. Wang and B. M. Klein, Phys. Rev. B **24**, 3417 (1981).
[62] H. J. Monkhorst and J. D. Pack, Phys. Rev. B **13**, 5188 (1976).
[63] A. J. Read and R. J. Needs, Phys. Rev. B **44**, 13071 (1991).
[64] B. Adolph, V. I. Gavrilenko, K. Tenelsen, F. Bechstedt, and R. Del Sole, Phys. Rev. B **53**, 9797 (1996).
[65] *Semiconductors Data Handbook*, edited by O. Madelung, 3rd ed. (Springer-Verlag, Berlin, 2004).
[66] *Handbook of Optical Constants of Solids*, edited by E. D. Palik, (Academic, London, 1998).
[67] M. A. Mojumder, Solid State Commun. **43**, 13 (1982).
[68] D. G. Thomas and J. J. Hopfield, Phys. Rev. **116**, 573 (1959).
[69] J.-B. Xia, Phys. Rev. B **38**, 8358 (1988).
[70] C.-Y. Yeh, S. B. Zhang, and A. Zunger, Phys. Rev. B **50**, 14405 (1994).
[71] W. J. Fan, J. B. Xia, P. A. Agus, S. T. Tan, S. F. Yu, and X. W. Sun, J. Appl. Phys. **99**, 013702 (2006).
[72] J. R. Chelikowsky and M. L. Cohen, Phys. Rev. B **14**, 556 (1976).
[73] F. Herman and S. Skillman, *Atomic Structure Calculations* (Prentice-Hall, Englewood Cliffs, N J, 1963).
[74] Z. Zanolli, M.-E. Pistol, L. E. Froberg, and L. Samuelson, J. Phys. Condens. Matter **19**, 295219 (2007).
[75] K. Shimada, T. Sota, and K. Suzuki, J. Appl. Phys. **84**, 4951 (1998).
[76] C.-Y. Yeh, Z. W. Lu, S. Froyen, and A. Zunger, Phys. Rev. B **46**, 10086 (1992).